

Interband resonant tunneling and transport in InAs/AlSb/GaSb heterostructures

Maria A. Davidovich

*Departamento de Física, Pontifícia Universidade Católica do Rio de Janeiro,
Caixa Postal 38071, 22452 Rio de Janeiro, Rio de Janeiro, Brazil*

E. V. Anda

*Instituto de Física, Universidade Federal Fluminense, Outeiro de São João Batista,
20420 Niterói, Rio de Janeiro, Brazil*

C. Tejedor

Departamento de Física de la Materia Condensada, Universidad Autónoma de Madrid, Cantoblanco, 28049 Madrid, Spain

G. Platero

*Instituto de Ciencia de Materiales (Consejo Superior de Investigaciones Científicas), Madrid, Spain
(Received 20 April 1992)*

The nonequilibrium Green-function Keldysh formalism is used to analyze resonant interband tunneling in double-barrier structures and nonresonant interband transport in polytype heterostructures of InAs, GaSb, and AlSb. The systems are modeled by a multiband tight-binding Hamiltonian that incorporates mixing of electron, light-hole, and heavy-hole states. The model is solved by the real-space renormalization technique, which is very rapid and numerically stable for any size of the system. The large difference in effective masses and the opposite curvature of the energy dispersion of the conduction band in InAs and valence bands in GaSb are reflected in the transport properties. The I - V characteristics of double-barrier structures show quite different features according to whether the well is InAs or GaSb. For the latter case, the current intensity peaks and the peak-to-valley current ratios are much larger than for the former case. The calculated I - V characteristics are generally in very good agreement with the experimental data. The density of states and the dispersion relation of the resonant states as a function of the in-plane wave vector are also discussed.

I. INTRODUCTION

Resonant tunneling in semiconductor heterostructures has been extensively investigated due to its potential application in high-speed electronic devices. Recent advances in epitaxial growth made possible the fabrication of a variety of devices, based on the polytype combination InAs/AlSb/GaSb (Refs. 1–7), which have shown high-frequency response and peak-to-valley current ratios larger than any previously reported for tunnel structures. This high performance is due to an electronic transport mechanism that, unlike the conventional GaAs/AlGaAs double-barrier structure, involves interband tunneling between conduction- and valence-band states. The valence-band edge of GaSb is about 0.15 eV higher in energy than the conduction-band edge of InAs.

From the theoretical point of view transport properties in mesoscopic systems have been investigated using different formalisms and approximations for a variety of conditions related to temperature, external fields, dimension, disorder, and many-body interactions. Resonant tunneling has been considered either as a scattering problem incorporating many-body effects through the calculation of the transmission matrix that implies the knowledge of two-particle Green's functions,⁸ or using the tunneling Hamiltonian formalism.⁹ Although these studies represent a significant contribution to the under-

standing of tunneling where multiphonon processes are considered, it is difficult to apply them to real systems. These approaches treat the tunneling in an extremely simplified way, describing the system by one state, the resonant state, interacting with connecting leads.

Within the one-body approximation the envelope-function formalism has been used in the study of resonant tunneling. However, this approach provides results for the current peak-to-valley ratio much larger than the ones measured in real systems. Besides, it is not suitable to treat more complex systems where band mixing is important such as the X -point tunneling in GaAs/AlGaAs and the interband transport in polytype heterostructures, the problem we are addressing in this paper.

Recently, multiband tight-binding models together with the transfer-matrix approach have been applied to resonant tunneling in GaAs/AlAs (Ref. 10) and to the interband transport in some polytype heterostructures.¹¹ In these studies the difficulties due to the numerical instabilities appearing in the transfer-matrix method¹² when applied to large systems have been overcome. In both the current density is obtained through the calculation of transmission coefficients. The peak-to-valley current ratios predicted in Ref. 10 are more realistic than the ones obtained by the envelope-function approximation. In Ref. 11 multiband and two-band model results are compared and the band mixing between heavy and light holes

is discussed. However no comparison with the experimental results is made.

In this paper we carry through an extensive discussion of the features of the current density-voltage (I - V) characteristics for a variety of interband transport devices and for the first time we present realistic theoretical results for interband resonant tunneling in double-barrier structures. The Keldysh formalism¹³ for nonequilibrium systems is applied to heterostructures represented in a tight-binding basis. This approach has already been applied by the authors to study interband tunneling within a two-band model,¹⁴ including only interactions between the conduction and the light-hole bands. It has also been used to study inelastic scattering processes in conventional resonant tunneling.¹⁵ Within the spirit of the bond-orbital model¹⁶ the Hamiltonian parameters are obtained from a reformulation of the Kane's $\mathbf{k}\cdot\mathbf{p}$ model, previously proposed¹⁷ by the authors, which takes fully into account the interactions among the conduction band and the heavy- and light-hole bands. To treat the nonequilibrium situation created by the application of a finite voltage to the heterostructures we follow the ideas proposed by Caroli *et al.*¹⁸ in their study of the tunneling through insulating barriers. The nonequilibrium Green functions are calculated by the real-space renormalization technique, which has shown to be very rapid and numerically stable for any size of the system. The Keldysh formalism has several advantages compared to other methods. The study of the transport properties within this formulation requires the calculation of one-particle Green functions, even when considering many-body effects. In other approaches the study of these effects needs the knowledge of two-particle Green functions which are commonly more involved to be calculated. In the independent particle situation Keldysh treatment gives exact results and in the case of correlated systems the physical properties can be calculated, in principle, to all orders in perturbation theory. Moreover, unlike other methods, it provides the occupation spectra at each point of the sample. This gives useful information about the existence of hot electrons in the system and contributes to the understanding of the range of validity of concepts like quasi-Fermi level and quasiequilibrium, which are used in the semi-phenomenological approaches based on the Landauer formula¹⁹ for the electrical current. The Keldysh formalism is also suitable to study the multistability present in tunneling current measurements²⁰ by treating self-consistently the potential profile produced by the external bias. In a situation in which many-body effects can be neglected the Keldysh formalism is exact and gives the same results for the I - V characteristics as the transfer-matrix approach and the Landauer formalism. However it gives more complete information about the transport process.

We apply this theoretical approach to study interband transport in polytype heterostructures composed by InAs, AlSb, and GaSb in a variety of configurations for which experimental data is available. The InAs/GaSb band line up is of the type II with the top of the valence band of GaSb 0.15 eV higher than the bottom of the InAs conduction band, leading to the possibility of interband

transport through the interface. When a thin layer of a large gap material such as AlSb is intercalated between them, forming a single barrier structure, electrons can tunnel from the InAs conduction band to the GaSb valence band resulting in interband tunneling. In both cases in spite of the absence of any confinement, the I - V characteristic curves present negative differential resistance, which is a consequence of the opposite curvature of the energy dispersion of the conduction and valence bands. Resonant interband tunneling occurs when a double barrier is formed by intercalating two AlSb layers between GaSb and InAs. In this case, according to the material in the middle the resonant states in the well are electronlike or holelike. The I - V characteristic for each of these situations presents quite distinct behavior, mainly due to differences in the carrier effective masses of the materials at the well and at the electrodes. These differences are also reflected in the density of states as a function of the parallel wave vector k_{\parallel} and in the energy dispersion relations, which are also discussed in this paper. The results we obtain compare well with the experimental data available.

We consider only coherent transport, neglecting any scattering mechanisms. The band bending due to charge accumulation is also not taken into account and the electric potential profile is assumed to be a linear interpolation between the higher and the lower reservoir potentials. Under these circumstances the calculation of the current is exact.

In Sec. II we present the Keldysh formalism in the one-body approximation and the model Hamiltonian, which we use to describe the polytype InAs/AlSb/GaSb heterostructures. The results and comparison with experimental data available are presented in Sec. III. A summary is given in Sec. IV.

II. THEORETICAL FORMALISM

A. Model Hamiltonian

The heterostructure is modeled by a Hamiltonian represented in a tight-binding basis, which is the adequate set of functions to apply the Keldysh formalism for nonequilibrium spatially heterogeneous systems. In order to describe interband transport processes the model should incorporate the conduction and valence bands and their interactions. The basis taken consists of three orbitals per site and spin: s states $|s = \frac{1}{2}, m_s = \pm \frac{1}{2}\rangle$ and the four states $|j = \frac{3}{2}, m_j = \pm \frac{3}{2}\rangle$ and $|j = \frac{3}{2}, m_j = \pm \frac{1}{2}\rangle$, giving rise to the conduction and the heavy- and light-hole bands, respectively. The lower spin-orbit-split band lies too low in energy to play any significant role in transport since the carriers involved have energies near the bottom of the conduction band and the top of the upper valence bands. In this basis the Hamiltonian can be written

$$\mathcal{H} = \sum_{\alpha, \beta}^{i, j} V_{ij}^{\alpha\beta} C_i^{\alpha\dagger} C_j^{\beta}, \quad (1)$$

where α, β stand for the orbitals and i, j for the sites, which we consider for simplicity to be in a simple cubic

lattice. The $V_{ij}^{\alpha\beta}$ parameters are chosen to reproduce, for the bulk material, the Kane's $\mathbf{k}\cdot\mathbf{p}$ Hamiltonian²¹ when a Fourier space transformation is performed in (1). This ensures that the tight-binding Hamiltonian we use reproduces, for the bulk, the dispersion relations of the zinc-blend structure.

Following Ref. 22 we adopt the cylindrical approximation to Kane's Hamiltonian and we choose the x axis along the heterostructure growth direction and the y axis

$$\begin{pmatrix} Ec + \frac{(k_x^2 + k_{\parallel}^2)}{2} & -iP(k_x - ik_{\parallel})/\sqrt{6} & iP(k_x + ik_{\parallel})/\sqrt{2} \\ iP(k_x + ik_{\parallel})/\sqrt{2} & Ev - \frac{\gamma_1 - \bar{\gamma}}{2}(k_x^2 + k_{\parallel}^2) & \sqrt{3}\bar{\gamma}(k_x - ik_{\parallel})^2/2 \\ -iP(k_x - ik_{\parallel})/\sqrt{2} & \sqrt{3}\bar{\gamma}(k_x + ik_{\parallel})^2/2 & Ev - \frac{\gamma_1 + \bar{\gamma}}{2}(k_x^2 + k_{\parallel}^2) \end{pmatrix}, \quad (2)$$

where Ec is the bottom of the conduction band, Ev the top of the valence bands, P is the Kane's momentum matrix element and γ_1 and $\bar{\gamma}$ ($\bar{\gamma} = \gamma_2 = \gamma_3$) are the Luttinger valence-band parameters.

In order to obtain (2) by Fourier transforming the Hamiltonian (1), it is sufficient to consider first-neighbor hoppings only, except in the case of the matrix elements between states $|2\rangle$ and $|3\rangle$, where second-neighbor interactions have also to be considered.

Comparing the Fourier transform of (1) with (2) we obtain the tight-binding matrix elements $V_{ij}^{\alpha\beta}$ in terms of the Kane's Hamiltonian parameter, which are known for the bulk materials. These are shown in Table I and Fig. 1.

The tight-binding Hamiltonian so obtained is applied to study a variety of heterostructure configurations. At the interfaces, the interactions linking the two parts of the system are taken to be the geometrical averages of their values at the materials on each side.

Due to the in-plane translational symmetry the k_{\parallel} wave vector is a good quantum number. Taking the Fourier transform in this plane the Hamiltonian (1) can

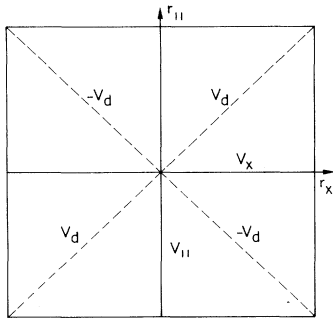


FIG. 1. Representation of the tight-binding hopping parameters. V_x and V_{\parallel} are the first-neighbor interactions along the heterostructure growth direction r_x and the in-plane direction r_{\parallel} , respectively. V_d is the second-neighbor interaction between states $|2\rangle$ and $|3\rangle$ defined in the text.

along the in-plane k_{\parallel} wave vector ($k_z=0$). This choice leads to the decoupling of the 6×6 matrix Hamiltonian into two equivalent 3×3 matrices; one block corresponding to the set of there state $|1\rangle = |(s = \frac{1}{2}, m_s = \frac{1}{2})\rangle$, $|2\rangle = |(j = \frac{3}{2}, m_j = -\frac{1}{2})\rangle$, and $|3\rangle = |(j = \frac{3}{2}, m_j = \frac{3}{2})\rangle$, and the other block corresponding to the opposite spin set. The Hamiltonian in this shorter basis retains the full coupling of electrons, heavy holes, and light holes and can be written (in atomic units) as

be written as

$$\mathcal{H} = \sum_{k_{\parallel}} \sum_{ij} t_{ij}(k_{\parallel}) C_i^{k_{\parallel}\dagger} C_j^{k_{\parallel}}, \quad (3)$$

where i, j stand for the layer position along the growth direction and the matrix elements of t_{ij} are the Fourier transform of the $V_{ij}^{\alpha\beta}$ along k_{\parallel} .

B. Nonequilibrium formalism

The current circulating along a sample when finite external bias is applied is a nonlinear response phenomenon occurring in a system which is in nonequilibrium. In view of the irreversible character of the tunneling current, the usual perturbation theory does not apply and it is necessary to use a more general formalism capable of treating nonequilibrium processes. We adopt Keldysh¹³ diagrammatic perturbation, which requires the definition of a state of zero current flow that is obtained by partitioning the system at an arbitrary point such that each partition (left and right) has a Fermi level defined by E_{f_L} and E_{f_R} , where the difference $E_{f_L} - E_{f_R}$ corresponds to the external applied voltage. This state is then used to build up an infinite diagrammatic expansion taking as a perturbation the Hamiltonian that connects the two parts of the system. The diagrammatic expansion generated by this perturbation theory can be summed up without further difficulties and an exact result obtained as far as a single-particle system is concerned. The effect of the interaction between particles (electron-electron and electron-phonon interaction) can be incorporated in principle in the theory using well-known approximations provided by many-body theory. However in this paper we restrict ourselves to an independent particle description.

In order to obtain the properties of the system it is necessary to calculate nonequilibrium propagates which, following Keldysh formalism, are

$$-iG_{ij}^{-+}(t-t') = \langle c_i^{\dagger}(t)c_j(t') \rangle, \quad (4a)$$

$$iG_{ij}^{+-}(t-t') = \langle c_j(t')c_i^{\dagger}(t) \rangle. \quad (4b)$$

TABLE I. The tight-binding matrix elements. $\alpha, \beta = 1, 2, 3$ are the three states defined in the text. P is Kane's momentum matrix element, γ_1 and $\bar{\gamma}$ the Luttinger parameters, and a the lattice constant. ϵ is the diagonal matrix element. For definition of $V_x, V_{\parallel},$ and V_d see Fig. 1.

| $\alpha=1, \beta=1$ | $\alpha=2, \beta=2$ | $\alpha=3, \beta=3$ | $\alpha=1, \beta=2$ | $\alpha=2, \beta=1$ | $\alpha=1, \beta=3$ | $\alpha=3, \beta=1$ | $\alpha=2, \beta=3$ | $\alpha=3, \beta=2$ | $\alpha=2, \beta=3$ |
|---|--|--|-------------------------------|------------------------------|-------------------------------|-------------------------------|------------------------------|-------------------------------|--|
| $\epsilon = E_c - \frac{2\hbar^2}{m_e^* a^2}$ | $\epsilon = E_v - \frac{2(\gamma_1 - \bar{\gamma})}{a^2}$ | $\epsilon = E_v - \frac{2(\gamma_1 + \bar{\gamma})}{a^2}$ | $V_x = -\frac{P}{2\sqrt{6}a}$ | $V_x = \frac{P}{2\sqrt{6}a}$ | $V_x = -\frac{P}{2\sqrt{6}a}$ | $V_x = -\frac{P}{2\sqrt{2}a}$ | $V_x = \frac{P}{2\sqrt{2}a}$ | $V_x = -\frac{P}{2\sqrt{2}a}$ | $V_x = -\frac{P}{2\sqrt{2}a}$ |
| $V_x = V_{\parallel} = -\frac{\hbar^2}{2m_e^* a^2}$ | $V_x = V_{\parallel} = \frac{\gamma_1 - \bar{\gamma}}{2a^2}$ | $V_x = V_{\parallel} = \frac{\gamma_1 + \bar{\gamma}}{2a^2}$ | $V_{\parallel} = -iV_x$ | $V_{\parallel} = -iV_x$ | $V_{\parallel} = -iV_x$ | $V_{\parallel} = iV_x$ | $V_{\parallel} = iV_x$ | $V_{\parallel} = iV_x$ | $V_d = i\frac{\sqrt{3}\bar{\gamma}}{4a^2}$ |

The Fourier transforms of the diagonal elements $G_{ii}^{-+}(\omega)$ and $G_{ii}^{+-}(\omega)$ are the spectral representations of the state of occupation of site i for electrons and holes, respectively. The retarded and advanced Green functions $G_{ij}^r(t-t')$ and $G_{ij}^a(t-t')$ give information on the distribution of available states of the system without any references to their occupation.

The propagators $G_{ij}^{-+}(\omega)$ and $G_{ij}^r(\omega)$ satisfy Dyson-type equations

$$G_{ij}^{-+}(\omega) = \{ [1 + G^r(\omega)\Sigma^r(\omega)] g^{-+}(\omega) \times [1 + \Sigma^a(\omega)G^a(\omega)] \}_{ij}, \quad (5a)$$

$$G_{ij}^r(\omega) = g_{ij}^r(\omega) + [g^r \Sigma^r(\omega) G^r(\omega)]_{ij}. \quad (5b)$$

Similar equations are satisfied by $G_{ij}^{+-}(\omega)$ and $G_{ij}^a(\omega)$. The unperturbed propagators $g_{ij}(\omega)$ correspond to two isolated subsystems in thermodynamical equilibrium, which are obtained by disconnecting two subsequent sites (1 and 2 in Fig. 2) of the original system. $g_{ij}^{-+}(\omega)$ and $g_{ij}^{+-}(\omega)$ are simply given by

$$g_{ij}^{-+}(\omega) = i \text{Im} g_{ij}^r(\omega) \begin{Bmatrix} f(\omega) \\ 1 - f(\omega) \end{Bmatrix}, \quad (5c)$$

where $f(\omega)$ is the Fermi distribution function.

The retarded and advanced matricial objects $\Sigma_{1,2}^r(\omega)$ and $\Sigma_{1,2}^a(\omega)$ correspond to local time one-particle self-energies that reconstitute the eliminated connection between sites 1 and 2, reestablishing the nonequilibrium situation. In our case they are simply the hopping matrix t_{12} .

The total current crossing the sample is obtained as the thermodynamical nonequilibrium mean value of the current operator. This can be obtained by calculating the probability of an electron to hop from site i to site $i+1$ minus the probability of having the reverse process. As there are no sources or sinks of electrons in the system the result is independent of the particular choice of site i . For the Keldysh formalism this is true if the perturbation expansion from the state for which the system is partitioned is done to all orders of perturbation theory, as in the case of the single particle system we are considering. The choice, being a matter of convenience, is made at the

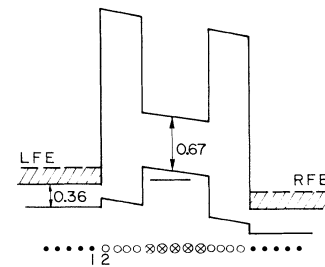


FIG. 2. Energy-band diagram of a double-barrier polytype heterostructure with GaSb as the well and n -doped InAs as the electrodes, under applied bias. LFE and RFE are the Fermi energies at the left and at right. The different planes of atoms are represented as follows: full circles, InAs; open circles, AlSb; and crossed circles, GaSb. The current density is calculated between planes 1 and 2.

contact between the left lead and the heterostructure involving the sites 1 and 2 shown in Fig. 2. The mean value of the current is then given by

$$J = \frac{ie}{\hbar} t_{12} (\langle c_{1\sigma}^\dagger c_{2\sigma} \rangle - \langle c_{2\sigma}^\dagger c_{1\sigma} \rangle), \quad (6)$$

where sites 1 and 2 are linked by the one-particle hopping t_{12} .

In order to calculate the nonequilibrium mean values appearing in Eq. (6) we apply the formalism presented in this section. After some algebra, using Eqs. (5) and (6) the total current can be obtained as

$$J = \frac{et_{12}^4}{2\pi\hbar} \int g_{11}^{-+}(\omega) g_{22}^{+-}(\omega) |G_{1,2}^r(\omega)|^2 d\omega. \quad (7)$$

The integration in Eq. (7) is restricted to the interval $Ef_L - Ef_R$ as it is evident from Eq. (5c). This guarantees that the current is zero when there is no external applied bias.

III. GaSb-InAs-AlSb HETEROSTRUCTURES: RESULTS AND DISCUSSIONS

We now apply the theoretical approach presented in the last section to study polytype heterostructures constituted by InAs, GaSb, and AlSb in different configurations for which experimental data are available. In our calculations we use InAs/GaSb and GaSb/AlSb valence-band offset values of 0.51 eV (Ref. 23) and 0.40 eV (Ref. 24), and gap values of 0.36, 0.67, and 2.2 eV for InAs, GaSb, and AlSb, respectively. The origin of the energy scale is taken at the top of the InAs valence band.

A. Double-barrier structures: EHE tunneling

In Fig. 2 the band structure of a double-barrier system constituted by AlSb barriers and a GaSb well connected to n -doped InAs electrodes is schematically illustrated. Tunneling of electrons from one electrode to the other via the quantized hole state of the well occurs when applied voltage is such that a resonant-state energy in the GaSb well coincides with the energies of the electrons in one of the InAs electrodes. We denote this process by electron-hole-electron (EHE) tunneling. In the inverse case where the roles of GaSb and InAs are interchanged we call the process a hole-electron-hole (HEH) tunneling and it will be discussed later.

As a first example we consider an asymmetric double barrier with the dimensions of one of the samples reported in Ref. 2: 100-Å GaSb well and 15-Å- and 25-Å AlSb barriers. In Fig. 3 the local density of states (LDOS), calculated at site 2 (Fig. 2) is shown for $k_{\parallel} = 0.00, 0.01,$ and 0.02 and without external bias. Throughout this paper k_{\parallel} is given in units of $2\pi/a$, where a is an average lattice parameter for the three materials and the sizes of the barriers and wells are approximated since they are constituted by integer numbers of layers. For $k_{\parallel} = 0.0$, over the range of energy of interest for interband tunneling $0.36 \text{ eV} \leq \varepsilon \leq 0.51 \text{ eV}$ there are five resonant hole states, the one at 0.424 eV being about ten times more intense than the others. This is a light-hole state with a small mixing of the s -states, as can be seen in Fig. 4 where the LDOS

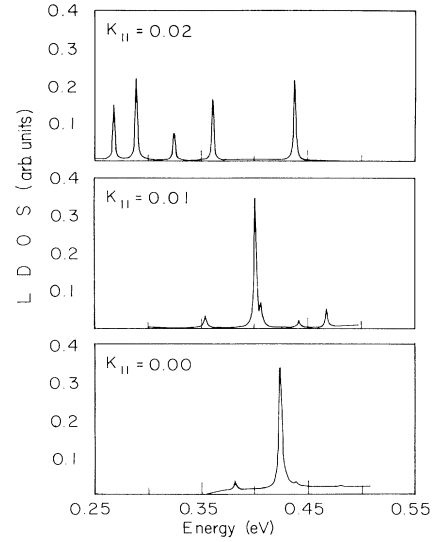


FIG. 3. Local density of states for InAs-AlSb-GaSb-AlSb-InAs double-barrier structure with no bias, $d_b = 15 \text{ \AA}$ and $d_w = 100 \text{ \AA}$ for $k_{\parallel} = 0.00, 0.01,$ and 0.02 . k_{\parallel} in units of $2\pi/a$.

projected on the electron (S), the light-hole (LH), and the heavy-hole (HH) states (PLDOS) is depicted for $k_{\parallel} = 0.00$ and 0.01 . Notice that, for clarity, the projections on the S and HH states are amplified, respectively, by factors of 3 and 5, with respect to the LH state. The other four states are pure HH states for $k_{\parallel} = 0.0$. As the value of k_{\parallel} is increased, the relative intensity of the peaks changes and the resonances move to lower energies as a consequence of the downward curvature of the energy dispersion in k_{\parallel} . The mixing induced by $k_{\parallel} \neq 0$ is clearly seen in Fig. 4, which shows all resonant states with contributions from the three components, although the LH state predominates. The energy dispersion relations for these states show anticrossings between heavy- and light-hole types of states, as represented in Fig. 5 for small values of k_{\parallel} .

The I - V characteristics for two polarities are presented in Fig. 6. By narrow-wide (NW) bias we mean the narrow barrier at the higher electric potential energy while wide-narrow (WN) bias corresponds to the opposite situation. The Fermi energy of 50 meV, consistent with a doping concentration of the order of $10^{17}/\text{cm}^3$, is chosen to locate the Fermi level just below the more intense resonance at 0.424 eV (Fig. 3). Due to conservation of k_{\parallel} , for this Fermi energy the maximum value of k_{\parallel} that contributes to the current is ≈ 0.01 and the tunneling involves predominantly a LH state.

The peak of the I - V curve for the NW bias case occurs at 0.04 V and has the intensity of 520 A/cm² while for the WN bias case it appears at 0.03 V with an intensity of 150 A/cm², 3.5 times smaller. This is expected since in the NW bias case as the bias is increased the wide barrier gets lower than the narrow one, making them equivalent at the resonance condition. This symmetric situation maximizes tunneling. These predicted values compare well with the data reported in Ref. 2, which shows the

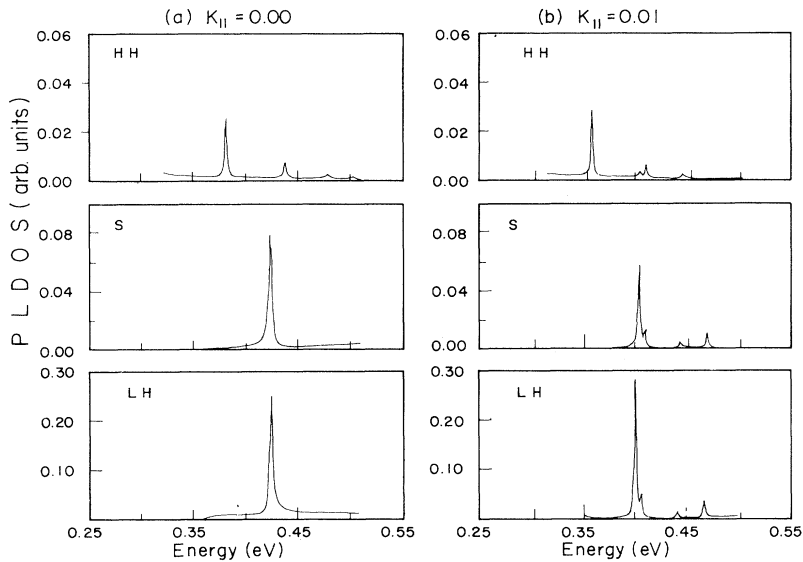


FIG. 4. Local density of states projected on the S, LH, and HH states for the same structure as in Fig. 3 and (a) $k_{||}=0.00$ and (b) $k_{||}=0.01$. $k_{||}$ in units of $2\pi/a$. For clarity the vertical scales are different so that the S-state intensity is multiplied by a factor of 3 and the HH state by a factor of 5, relative to the intensity of the L-H state.

I - V characteristic for the WN bias case, at low temperature, with a peak at about 0.04 V and intensity about 110 A/cm², six times smaller than the intensity for the NW bias case. Also observed² are larger values for the peak-to-valley current ratios in the WN bias case ($P/V=88$) than in the NW bias case ($P/N=28$). An inspection of Fig. 6 shows that our curves also present this tendency. Although it is difficult to predict a value for P/V from our results due to the every flat current valley, we make a rough estimate, taking average values over some points in the current valley obtaining approximately $P/N=110$, and 70 for the WN and NW bias case, respectively, following the correct trend. These values are larger than the measured ones probably because our calculations neglect electron-phonon scattering processes that tend to decrease the peak and to increase the valley of the I - V curves.

The general triangular shape of the I - V characteristics also agrees well with the experimental result and is opposite to the one observed in the traditional GaAs/AlAs double-barrier structures. The sharp increase of the current for small voltages is due to the high density of states at the energy for which the resonance level coin-

cides with the Fermi level. The different effective masses and the opposite curvature of the energy dispersion in the GaSb well and InAs electrodes contribute also to the fast raise. The voltage at which a maximum number of $k_{||}$ values contributes to the current corresponds to the one which aligns the well quantum level with the Fermi energy at the left electrode. The effect of the difference between the electronic effective masses of the electrodes and the well has been discussed and observed²⁵ for the X -point tunneling in GaAs/AlAs double-barrier structures.

We have also considered (not shown) EHE tunneling in an asymmetric double-barrier structure with 65 Å GaSb well for which experimental results are also reported in Ref. 2. We find in this case the same trend as before. The calculated current peaks for the NW bias case (290 A/cm²) and for the WN bias case (60 A/cm²) are smaller than the ones obtained for the 100 Å GaSb well. The WN bias case presents also a larger peak-to-valley current ratio. These features are also in agreement with the experimental data.²

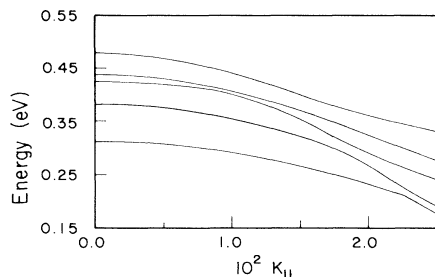


FIG. 5. Energy dispersion relation in $k_{||}$ for the five resonant states shown in Fig. 3. $k_{||}$ in units of $2\pi/a$.

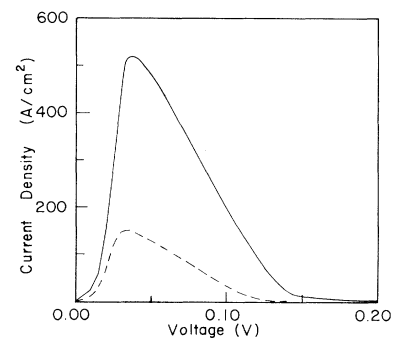


FIG. 6. I - V characteristic for EHE tunneling in asymmetric double-barrier structure with $d_b=15$ and 25 Å and $d_w=100$ Å. The Fermi energy is 50 meV. NW bias (solid line), WN bias (dashed line). Set text for definition of NW and WN.

B. Double-barrier structures: HEH tunneling

The HEH tunneling, as mentioned before, occurs in double-barrier structures constituted by AlSb barriers and a InAs well connected to *p*-doped GaSb electrodes. An applied voltage that aligns the energies of the holes in one of the electrodes with the energy of a resonant state in the well produces tunneling of holes between the electrodes via the quantized electron state of the well.

To analyze this process we consider a symmetric double-barrier structure with a InAs well of 150 Å, for which the *I-V* characteristic curve has been measured.²⁶ In Fig. 7 we present the LDOS calculated at the one extremity of the structure for $k_{\parallel}=0.000$, 0.005, and 0.010 and no external bias. The density of states looks quite different from the one shown for EHE tunneling case. The contributions from the well quantum level and from the valence band of the electrodes are comparable. Moreover, within the range of energy of interest, as far as hole interband tunneling is concerned there is only one resonance, the first confined state of the well at 0.46 eV. The large resonance energy splittings in this well are due to the small effective mass in InAs and to the large InAs/AlSb conduction-band offset. Therefore, to obtain resonant tunneling the width of the InAs well cannot be too small. We predict the inferior limit to be about 120 Å, for which the first resonant state energy is at 0.51 eV, which coincides with the energy at the top of the valence band of the GaSb electrodes. On the other hand it is possible to obtain resonant tunneling in quite wide InAs wells, which makes this structure very attractive as far as the development of three terminal devices is concerned.

Another consequence of the small effective mass in the well is the large shift, compared to the EHE tunneling case, of the resonance peaks towards higher energies as k_{\parallel} increases, shown in Fig. 7. For $k_{\parallel}=0.01$ the resonance energy is already inside the gap region of the electrodes, too high to participate in the interband tunneling.

The resonant state, for $k_{\parallel}=0.0$, is a mixture of *S* and LH states as can be seen in Fig. 8, which shows the projected LDOS on the *S*, LH, and HH states. The mixing for $k_{\parallel}\neq 0$ with the HH state is negligible and consequently it does not appear in Fig. 8 for $k_{\parallel}=0.01$. The energy dispersion for the resonant state as a function of k_{\parallel} has an approximate parabolic shape. These features of the

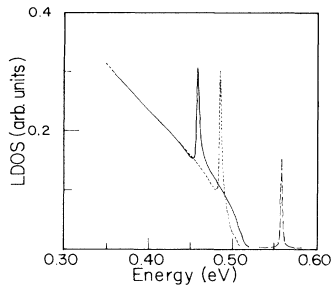


FIG. 7. Local density of states for GaSb-AlSb-InAs-AlSb-GaSb double-barrier structure with no bias, $d_b=15$ Å and $d_w=150$ Å, for $k_{\parallel}=0.000$ (solid line), $k_{\parallel}=0.005$ (dotted line), and $k_{\parallel}=0.010$ (dashed line) k_{\parallel} in units of $2\pi/a$.

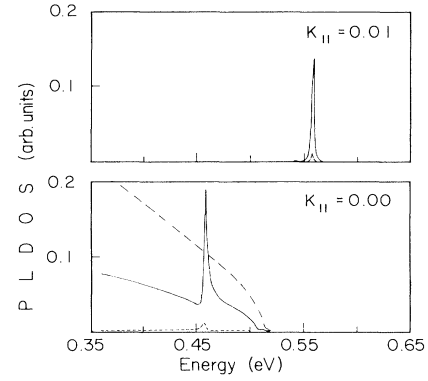


FIG. 8. Local density of states projected on the *S* state (dotted line), the LH state (solid line), and the HH state (dashed line), for the same structure as in Fig. 7, for $k_{\parallel}=0.00$ and $k_{\parallel}=0.01$. The HH state does not appear for $k_{\parallel}=0.01$ because it has a negligible contribution.

density of states are reflected on the shape of the *I-V* characteristics for the HEH tunneling.

Figure 9 shows the *I-V* characteristic for a 150-Å InAs well and Fermi energy of 5 meV, consistent with a *p*-doping concentration of about $10^{17}/\text{cm}^3$ in the GaSb electrodes, the same parameters used in Ref. 26. Notice that, although the resonant state of the well is 45 meV below the Fermi level, the current begins to rise for any finite voltage. Moreover, it keeps monotonically increasing after the minimum of the current density is reached. This contribution to the current comes essentially from a nonresonant tunneling that is comparable to the resonant one, as can be inferred from the density of states shown in Figs. 7 and 8. As a consequence, the HEH tunneling presents a low peak-to-valley current ratio, as compared to the EHE tunneling case, and the peak intensities are much smaller. Another consequence of the existence of a nonresonant current is that it deformats the intrinsically asymmetric shape of the peak, reducing the large negative slope of the upper bias side of the peak. This shape of the *I-V* characteristic compares quite well with the experiment,²⁶ although we find the peak position at lower voltages. This is probably due to the distortions of the

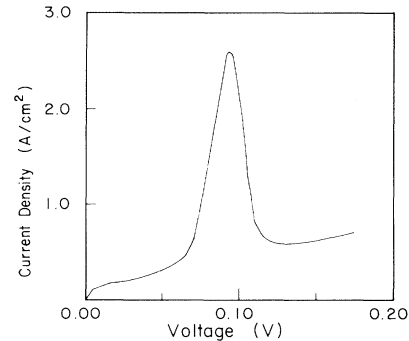


FIG. 9. *I-V* characteristic for the HEH tunneling with $d_b=15$ Å and $d_w=150$ Å. The Fermi energy is 5 meV.

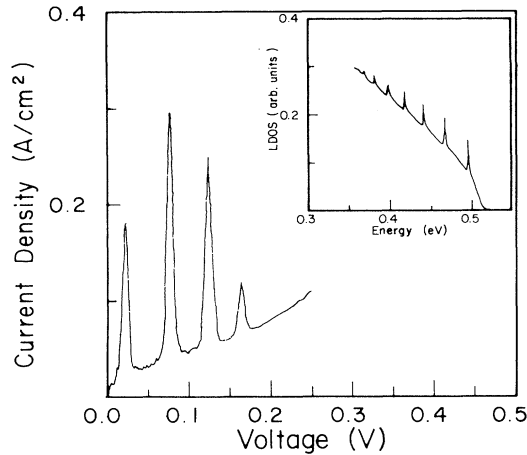


FIG. 10. I - V characteristic of the HEH tunneling with $d_w = 1100 \text{ \AA}$ and $d_b = 15 \text{ \AA}$ and Fermi energy of 2.5 meV. In the inset the density of states for no bias, for $k_{\parallel} = 0.0$.

potential profile caused by charge accumulation, which affects the position of the resonant state in the well and that has been disregarded in our calculation. The intensity in Ref. 26 is reported in arbitrary units.

To illustrate the possibility of resonant HEH tunneling in very wide quantum wells we present in Fig. 10 the I - V characteristic of a 1100- \AA InAs well, with Fermi energy of 2.5 meV. The inset shows the LDOS calculated at one extremity of the double-barrier structure.

C. Nonresonant interband transport: interface and single-barrier structure

The I - V characteristic for a single AlSb barrier of 27 \AA interjacent between n -doped InAs and p -doped GaSb electrodes and for the InAs/GaSb interface are presented in Figs. 11 and 12, respectively. In the latter case the external bias is applied over 20 layers of the material in each side of the interface. For both cases the doping is such as to locate the equilibrium Fermi level at 0.41 eV,

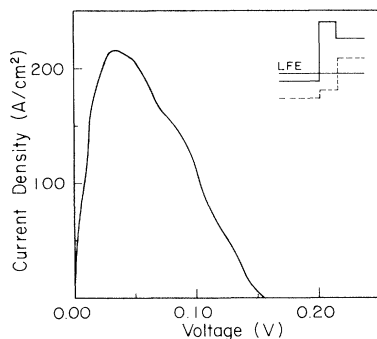


FIG. 11. I - V characteristic for a 27 \AA single barrier of AlSb, intercalated in the InAs/GaSb interface. The Fermi level (LFE) is at 0.41 eV as shown in the inset, where the energy-band diagram for no bias is illustrated.

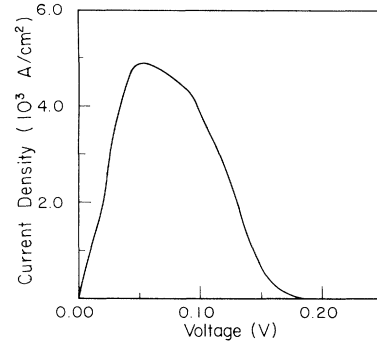


FIG. 12. I - V characteristic for the InAs/GaSb interface. The electrical potential is applied over 20 layers at each side of the interface. The Fermi level is at 0.41 eV, as in the case of the single barrier.

50 meV above the InAs conduction-band minimum. Since it is a nonresonant process the current density begins to rise for any finite applied bias and ceases when the top of the GaSb valence band crosses the bottom of the InAs conduction band, at about 0.15 V. Both curves show a sharp raise and slow decay because the values of the density of states involved in the transport are larger for lower bias. The peak intensity for the interface is 25 times larger than for the single barrier and it is higher than for any other system we have analyzed, due to the lack of a barrier. Because of the opposite curvatures of the energy dispersion the blocking of the current is very efficient. Therefore interfaces should present very high peak-to-valley current ratios. The experimental results,⁶ however, show high peak current densities, of about 10^4 A/cm^2 , but very low peak-to-valley current ratios. It is argued⁶ that the large values of the valley current are due to inelastic scattering processes that are not efficiently suppressed by the lack of a barrier.

IV. SUMMARY

We have studied resonant interband tunneling in double-barrier structures constituted by a well of GaSb (InAs) connected to electrodes of n -doped InAs (p -doped GaSb) through AlSb barriers. We have also analyzed the nonresonant interband transport through InAs/GaSb interface with and without an intercalating AlSb barrier.

The heterostructures are modeled by a Hamiltonian represented in a tight-binding basis of six orbitals (the lower spin-orbit-split band is neglected) whose parameters are obtained, with no fitting, from the Kane's $k \cdot p$ model. Within the cylindrical approximation adopted the Hamiltonian decouples into two equivalent 3×3 matrices. This makes the calculations much simpler and rapid, still retaining the full coupling of electron, heavy- and light-holes states.

The transport properties are obtained by the Keldysh formalism, which permits an adequate treatment of the nonequilibrium situation we are dealing with. The nonequilibrium Green functions are calculated by the real-space renormalization technique, which have shown to be

very rapid and numerically stable for any size of the system.

We have calculated the resonant interband tunneling in double-barrier structures for two configurations: either the carriers at the well are holes (EHE tunneling) or electrons (HEH tunneling). For these cases the density of states and the I - V characteristics show quite different features mainly due to differences in the effective masses of the electrons in InAs and holes in GaSb. In order to be able to compare with experimental data we have done calculations for structures with the same sizes as the ones measured. In both cases the shapes of the calculated I - V characteristics are in very good agreement with the experimental ones. The curves for EHE tunneling present a triangular shape opposite to the one shown for the more conventional GaAs/AlGaAs double-barrier structure. This is due to the different sign and value of the curvature of the energy dispersion relation of the hole resonant state of the well and the conduction band of the electrodes. As to the voltage and intensity of the peaks we predict the correct trends; for the asymmetric double-barrier structure the configuration at which the narrow barrier is at higher electric potential presents higher intensity peak and lower peak-to-valley current ratio than the opposite configuration, as has been reported.

The I - V characteristic of the HEH tunneling shows a resonant tunneling peak superposed to a nonresonant contribution that appears for any finite applied voltage. As a consequence the shape of the curve looks quite different from the one for the EHE tunneling and also the peak-to-valley current ratio is much smaller. Because of the small effective mass of the conduction-band electrons in InAs the HEH resonant tunneling can be obtained even for quite large wells. We illustrate this calculating the I - V characteristic for a InAs well of 1100 Å. We have also analyzed the mixing of the HH states with the S and LH states by studying the density of states project-

ed on these states.

As examples of nonresonant transport we have calculated the current through the InAs/GaSb interface with and without the intercalation of a AlSb barrier. As expected the current begins to increase for any applied bias and it goes to zero as the top of the valence band of GaSb crosses the bottom of the conduction band of InAs at about 0.15 V.

The Keldysh method has been shown to be a very powerful formalism to calculate the transport properties of a system under an applied external bias. The tight-binding representation of the Hamiltonian allows a more natural and better treatment of the interfaces, particularly appropriate for the case of superposition of conduction and valence bands, as opposed to the conventional envelope-function method. The influence of many-body effects, electron-electron, and electron-phonon interactions has been neglected in this work but they can be treated as a natural extension of our calculations, as already pointed out. The bistability, the accumulation charge effects, and the relaxation processes are currently being studied. We are also analyzing the effects of a magnetic field on the transport properties of interband devices.

ACKNOWLEDGMENTS

We would like to acknowledge partial support by the Conselho Nacional de Desenvolvimento Científico e Tecnológico of Brazil (CNPq), the Secretaria de Ciência e Tecnologia of Brazil (SCT/PR), and the Comision Interministerial de Ciencia y Tecnologia of Spain under Contract No. MAT88-0116-C02-01/02. Two of us (M.A.D. and E.V.A.) would like to acknowledge the hospitality of the Departamento de Física de la Materia Condensada, Universidad Autonoma de Madrid, Madrid, during a recent visit.

¹M. Sweeny and J. Xu, Appl. Phys. Lett. **54**, 546 (1989).

²J. R. Söderström, D. H. Chow, and T. C. McGill, Appl. Phys. Lett. **55**, 1094 (1989).

³L. F. Luo, R. Beresford, and W. I. Wang, Appl. Phys. Lett. **55**, 2023 (1989).

⁴R. Beresford, L. F. Luo, and W. I. Wang, Appl. Phys. Lett. **56**, 551 (1990).

⁵R. Beresford, L. F. Luo, K. F. Longenbach, and W. I. Wang, Appl. Phys. Lett. **56**, 952 (1990).

⁶D. A. Collins, E. T. Yu, Y. Rajakarunanayake, J. R. Söderström, D. Z.-Y. Ting, D. H. Chow, and T. C. McGill, Appl. Phys. Lett. **57**, 683 (1990).

⁷D. Z.-Y. Ting, D. A. Collins, E. T. Yu, D. H. Chow, and T. C. McGill, Appl. Phys. Lett. **57**, 1257 (1990).

⁸N. S. Wingreen, K. W. Jacobsen, and J. W. Wilkins, Phys. Rev. B **40**, 17, 11 834 (1989).

⁹M. Jonson, Phys. Rev. B **39**, 5924 (1989).

¹⁰T. B. Boykin, Jan P. A. van der Wagt, and J. S. Harris, Jr., Phys. Rev. B **43**, 4777 (1991).

¹¹D. Z.-Y. Ting, E. T. Yu, and T. C. McGill, Appl. Phys. **58**, 292 (1991); Phys. Rev. B **45**, 3583 (1991).

¹²J. N. Schulman and Y.-C. Chang, Phys. Rev. B **27**, 2346 (1983).

¹³L. V. Keldysh, Zh. Eksp. Teor. Fiz. **47**, 1515 (1964) [Sov. Phys.—JETP **20**, 1018 (1965)].

¹⁴Maria A. Davidovich, E. V. Anda, C. Tejedor, and G. Platero, in *Resonant Tunneling in Semiconductors: Physics and Applications*, edited by L. L. Chang, E. E. Mendez, and C. Tejedor (Plenum, New York, 1991), p. 61.

¹⁵E. V. Anda and F. Flores, J. Phys. Condens. Matter **3**, 9087 (1991).

¹⁶Y.-C. Chang, Phys. Rev. B **37**, 8215 (1988).

¹⁷Maria A. Davidovich, E. V. Anda, C. Tejedor, and G. Platero, in *The Physics of Semiconductors*, edited by E. M. Anastasakis and J. D. Joannopoulos (World Scientific, Singapore, 1991), p. 1649.

¹⁸C. Caroli, R. Combescot, P. Nozieres, and D. Saint-James, J. Phys. C **4**, 916 (1971).

¹⁹R. Landauer, J. Phys. C **1**, 8099 (1989).

²⁰P. L. Pernas, F. Flores, and E. V. Anda, J. Phys. Condens. Matter **4**, 5309 (1992).

²¹E. O. Kane, in *Semiconductors and Semimetals*, edited by R. K. Willardson and A. C. Beer (Academic, New York, 1966),

- Vol. 1, p. 75.
- ²²M. Altarelli, Phys. Rev. B **28**, 842 (1983).
- ²³G. J. Gaultieri, G. P. Schwartz, R. G. Nuzzo, R. J. Malik, and J. F. Walker, J. Appl. Phys. **61**, 5337 (1987).
- ²⁴G. J. Gaultieri, G. P. Schwartz, R. G. Nuzzo, and W. A. Sunder, J. Appl. Phys. **49**, 1037 (1986).
- ²⁵H. Ohno and E. E. Mendez, Appl. Phys. Lett. **56**, 1793 (1990).
- ²⁶E. E. Mendez, H. Ohno, L. Esaki, and W. I. Wang, Phys. Rev. B **43**, 5196 (1991).